

## Spontaneous emission of a quantum emitter near a graphene nanodisk under strong light-matter coupling

Ioannis Thanopoulos<sup>1</sup>, Vasilios Karanikolas<sup>2</sup>, and Emmanuel Paspalakis<sup>1</sup>

<sup>1</sup>*Materials Science Department, School of Natural Sciences, University of Patras, Patras 265 04, Greece*

<sup>2</sup>*International Center for Young Scientists (ICYS),*

*National Institute for Materials Science (NIMS) 1-1 Namiki, Tsukuba, Ibaraki 305-0044, Japan*



(Received 12 December 2021; accepted 11 July 2022; published 27 July 2022)

We investigate the dynamical evolution of the spontaneous emission of a two-level quantum emitter near a graphene nanodisk. We employ the macroscopic quantum electrodynamics methodology to study the reversible population dynamics of the excited state of the quantum emitter in the non-Markovian limit. Our results indicate that the quantum-emitter–nanodisk interaction enters the strong light-matter coupling regime, as manifested in the excited-state probability where Rabi oscillations and population trapping effects are observed. The level of non-Markovianity is estimated by computing three different well-established measures and relate them to the quantum speedup due to the strong-coupling interaction of the emitter with the graphene nanodisk. Importantly, high values of the non-Markovianity and quantum speedup measures are achieved when the emitter-nanodisk interaction is strong, whereas decreasing coupling strength leads to smaller values.

DOI: [10.1103/PhysRevA.106.013718](https://doi.org/10.1103/PhysRevA.106.013718)

### I. INTRODUCTION

In the area of quantum plasmonics the strong coupling between quantum emitters (QEs) and the modified electromagnetic field by plasmonic nanostructures has attracted significant interest in recent years due to several emerging applications in sensing, chemical reactivity, and quantum technology, among others [1–7]. In the time regime, the strong light-matter coupling manifests itself as reversible, non-Markovian, spontaneous emission dynamics of the QE. The QEs are usually combined with noble metal nanostructures (typically Au and Ag), that support surface plasmon modes to achieve the strong coupling regime; different nanostructures have been used, such as finite nanoparticles, metallic or metal-dielectric surfaces, as well as metallic and metal-dielectric cavities [8–25]. Additionally, the strong light-matter coupling effects in QEs near metallic nanostructures in the frequency regime have been observed in several important experiments [26–29].

Graphene is a two-dimensional material with important optical properties that also supports surface plasmons; it has been studied as an alternative for metallic nanostructures in nanophotonics [30,31]. The graphene surface plasmon modes lie in the near to far infrared part of the electromagnetic spectrum [32] and can be tuned by voltage gating, doping, or multilayer stacking. The interaction of QEs with light near graphene monolayers and graphene nanostructures is a topic of intense active research [32–57].

Among the graphene nanostructures, significant interest has been attracted to graphene nanodisks interacting with QEs by light [32–34,39,48,50,55]. The seminal work of Koppens *et al.* [32] showed that graphene nanodisk is an ideal platform for strong light-matter coupling; it can be used for quan-

tum optics at the single-photon level when a QE is placed near the graphene nanodisk. In particular, for the modeling of the light-matter interaction in this paper, they used a non-Hermitian Jaynes-Cummings Hamiltonian showing that significant vacuum Rabi splitting is possible in a QE near the graphene nanodisk. Furthermore, Manjavacas and co-workers have shown that a QE coupled to a graphene nanodisk structure can result to strong plasmon-plasmon interaction, leading to a plasmon blockade effect [34], as well as an enhancement of the quadrupolar transitions of QEs when located in the vicinity of the graphene nanodisk [48]. In addition, Karanikolas *et al.* have shown tunable and efficient long-range energy transfer between two QEs via a graphene nanodisk [39], whereas Cox *et al.* have studied the dipole-dipole interaction and energy transfer in a system consisting of a three-level QE and a graphene nanodisk embedded in a nonlinear photonic crystal [33] by analyzing the nonlinear optical response and coherent control in a strongly driven QE-graphene nanodisk structure [50]. More recently, Zeng and Zubairy studied surface-plasmon excitation in a graphene nanodisk using the transmission of a two-level QE in its ground state through the nanodisk [55].

Here, we explore the spontaneous emission dynamics of a QE near a graphene nanodisk. Thus, we investigate the non-Markovian behavior of the spontaneous emission dynamics of a QE placed near a graphene nanodisk using the macroscopic quantum electrodynamics approach [58], which we [59–61] and others [62] have used in investigating the spontaneous emission dynamics of a QE next to a MoS<sub>2</sub> nanodisk. More specifically, we perform electromagnetic calculations for the calculation of the Purcell factor and the spectral density for the QE near the graphene nanodisk; here, we note that the Purcell factors in the case of the graphene are about two orders of

magnitude larger than in the case of a MoS<sub>2</sub> nanodisk which allows for investigating the spontaneous emission dynamics of a QE under stronger light-matter interaction conditions than in the MoS<sub>2</sub> nanodisk case [59–61]. Then, we use these results in the integrodifferential equation for the probability amplitude of the excited state of the QE, which we solve numerically in order to obtain the QE spontaneous emission dynamics.

In our paper we go beyond the calculation of the population dynamics of the excited state of the QE by additionally analyzing the non-Markovian spontaneous emission dynamics using three widely used non-Markovianity measures, namely, the Breuer, Laine, and Piilo (BLP) measure [63] and the two measures proposed by Rivas, Huelga, and Plenio (RHP) [64]. In addition, we calculate the quantum speed limit presented in Ref. [65] for the evolution of the QE near the graphene nanodisk using the time evolution of the spontaneous emission.

In particular, we analyze the spontaneous emission dynamics of a QE modeled as a two-level system located at 5 and 15 nm from a graphene nanodisk of radius 30 nm, when the free-space decay time of the emitter lies between 100 ps and several microseconds. The population dynamics ranges from Markovian decay or weak non-Markovian response at long distances of the QE from the nanodisk and weak free-space decay rates to pronounced decaying Rabi oscillations or complex Rabi oscillations at shorter distances or for larger free-space decay rates. At short distances and even stronger free-space decay rates, population trapping in the excited state is also observed, which can be explained by the creation of a bound state, which lies in our case outside the photonic continuum [66,67]. These results are in agreement with the non-Markovianity measures and quantum speed limit calculations, which show large measure values and potentially large quantum speedup in the case of quantum dynamics under strong-coupling conditions, whereas both properties are decreasing as the coupling diminishes.

This paper is organized as follows: In Sec. II, we present the electromagnetic methodology for calculating the Purcell enhancement factors of a QE near a graphene nanodisk and the equation for the QE spontaneous emission dynamics. In Sec. III, we present the results for the excited-state population dynamics for two different distances of the QE from the center of the graphene nanodisk and for various free-space decay widths as well as the results for the different non-Markovianity measures and the quantum speed limit. We finally conclude our findings in Sec. IV.

## II. THEORY

In this section, we present the theory describing the relaxation of a two-level QE when placed nearby a graphene nanodisk with radius  $R$ . We consider a coordinate system with the origin at the center of the nanodisk, which coincides with

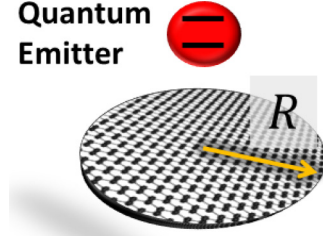


FIG. 1. Schematic of a two-level QE with transition frequency  $\omega_0$  in proximity to a graphene nanodisk of radius  $R$ .

the  $xy$  plane, and the QE is located above the disk center on the  $z$  axis, i.e., at  $\mathbf{r}_{\text{QE}} = (0, 0, z)$ , see Fig. 1.

Within the electric dipole and rotating-wave approximations, the total Hamiltonian of the system is written as [58] (we use  $\hbar = 1$  in this paper)

$$\begin{aligned} \hat{H} = & \omega_0 |1\rangle\langle 1| + \int d^3\mathbf{r}' \int_0^\infty d\omega \omega \hat{\mathbf{f}}^\dagger(\mathbf{r}', \omega) \cdot \hat{\mathbf{f}}(\mathbf{r}', \omega) \\ & + \int_{-\infty}^\infty d\omega \int d^3\mathbf{r}' \{g(\mathbf{r}', \omega) [\hat{\mathbf{f}}(\mathbf{r}', \omega) |1\rangle\langle 0| + \text{H.c.}]\}. \end{aligned} \quad (1)$$

Here,  $\omega_0$  is the transition energy of the QE, and  $\hat{\mathbf{f}}^\dagger(\mathbf{r}', \omega)$  and  $\hat{\mathbf{f}}(\mathbf{r}', \omega)$  denote the creation and annihilation bosonic vector field operators for the elementary excitations of the electromagnetic field, which obey the usual commutation relations [58]. Also,  $g(\mathbf{r}', \omega)$  is the coupling between the QE and the photonic field given by

$$g(\mathbf{r}', \omega) = -i \sqrt{\frac{1}{\pi \epsilon_0}} \frac{\omega^2}{c^2} \sqrt{\epsilon_I(\mathbf{r}', \omega)} \mathbf{G}(\mathbf{r}, \mathbf{r}', \omega) \boldsymbol{\mu}, \quad (2)$$

with  $\boldsymbol{\mu}$  being the transition dipole moment operator of the QE and  $\sqrt{\epsilon_I(\mathbf{r}', \omega)}$  denoting the imaginary part of the dielectric function. A crucial quantity, which describes the contribution of the modified nanophotonic environment, is the classical electromagnetic Green's tensor  $\mathbf{G}(\mathbf{r}, \mathbf{r}', \omega)$ . For the graphene disk considered here the electrostatic approximation is applied where the total Green's tensor is written as  $\mathfrak{G}(\mathbf{r}, \mathbf{r}', \omega) = \mathfrak{G}^0(\mathbf{r}, \mathbf{r}', \omega) + \mathfrak{G}^{\text{ind}}(\mathbf{r}, \mathbf{r}', \omega)$ ;  $\mathfrak{G}^0(\mathbf{r}, \mathbf{r}', \omega)$  is the homogeneous part of Green's tensor and  $\mathfrak{G}^{\text{ind}}(\mathbf{r}, \mathbf{r}', \omega)$  stands for the induced part of the Green's tensor accounting for the presence of the graphene nanodisk in the vicinity of the QE, which affects the coupling  $g(\mathbf{r}', \omega)$ .

The optical response of the graphene disk is described through its in-plane conductivity  $\sigma$ , which is calculated in the random-phase approximation [68,69]. It is expressed via the chemical potential  $\mu$  and the temperature  $T$ ,

$$\sigma = \sigma_{\text{intra}} + \sigma_{\text{inter}}, \quad (3)$$

where the intraband and interband contributions are [70]

$$\sigma_{\text{intra}} = \frac{2ie^2 k_B T}{\pi(\omega + i/\tau)} \ln \left[ 2 \cosh \left( \frac{\mu}{2k_B T} \right) \right], \quad (4a)$$

$$\sigma_{\text{inter}} = \frac{e^2}{4} \left[ \frac{1}{2} + \frac{1}{\pi} \arctan \left( \frac{\omega - 2\mu}{2k_B T} \right) - \frac{i}{2\pi} \ln \frac{(\omega + 2\mu)^2}{(\omega - 2\mu)^2 + (2k_B T)^2} \right]. \quad (4b)$$

The intraband term  $\sigma_{\text{intra}}$  describes the Drude-type response, which is corrected for scattering by impurities through a term containing  $\tau$ , the relaxation time. In this paper we consider room-temperature  $T = 300$  K, relaxation time of  $\tau = 1$  ps, and chemical potential  $\mu = 0.5$  eV [71].

Using an expansion of the charge density of the graphene disk over an appropriate set of functions,  $\rho(r) = \sum_{n=0}^{\infty} r^l c_n^l P_n^{(l,0)}(1 - 2r^2)$ , the induced part of the Green's tensor is calculated with  $l$  being the angular and  $n$  the radial eigenmode, and  $P_n^{(l,0)}$  standing for the Jacobi polynomials. Since we consider the QE placed above the center of the graphene disk,  $\mathbf{r} = (0, 0, z)$ , the induced part of the Green's tensor in the electrostatic regime [39,72] reads

$$\mathfrak{G}_{xx}^{\text{ind}}(\mathbf{r}, \mathbf{r}, \omega) = -\frac{c^2}{2\omega^2} \sum_{n=0}^{\infty} c_n^1(z, \omega) \frac{[Z(z, R) - z/R]^{2n+2}}{Z(z, R)}, \quad (5)$$

and

$$\mathfrak{G}_{zz}^{\text{ind}}(\mathbf{r}, \mathbf{r}, \omega) = \frac{\pm c^2}{2\omega^2} \sum_{n=1}^{\infty} c_n^0(z, \omega) \frac{[Z(z, R) - z/R]^{2n+1}}{Z(z, R)}, \quad (6)$$

where  $Z(z, R) = \sqrt{(z/R)^2 + 1}$  and  $c_n^l$ , ( $l = 0, 1$ ) are the expansion coefficients that yield the influence of the graphene disk on the dipole source with  $l = 1$  related to a QE with a transition dipole moment along  $x$  and  $l = 0$  when the transition dipole moment of the QE is along  $z$ .

The time-dependent state vector of the QE in proximity to the graphene nanodisk is given by

$$|\Psi(t)\rangle = c_1(t)e^{-i\omega_0 t}|1; 0_\omega\rangle + \int d\mathbf{r} \int d\omega c(\mathbf{r}, \omega, t)e^{-i\omega t}|0; 1_{\mathbf{r}, \omega}\rangle, \quad (7)$$

with  $|n; a\rangle = |n\rangle \otimes |a\rangle$ . Here, the vector  $|n\rangle$  ( $n = 0, 1$ ) represents the quantum states of the two-level QE, and  $|a\rangle$  describes the states of the modified photonic modes due to the presence of the graphene nanodisk. These photonic states have the form  $|0_\omega\rangle$ , describing the photonic vacuum (no photon excitation), and  $|1_{\mathbf{r}, \omega}\rangle$  describing the single-photon states (one-photon excitation). The probability amplitude  $c_1(t)$  is obtained by the solution of the integrodifferential equation [12],

$$\dot{c}_1(t) = i \int_0^t K(t - t')c_1(t')dt', \quad (8)$$

$$K(t - t') = ie^{i\omega_0(t-t')} \int_0^\infty J(\omega)e^{-i\omega(t-t')}d\omega, \quad (9)$$

with  $J(\omega) = \Gamma_0(\omega_0)\lambda^m(\omega, d)/2\pi$  ( $m = z, x$ ) being the spectral density of the electromagnetic mode continuum around the QE. Here,  $\Gamma_0(\omega_0)$  is the free-space decay rate of the QE with free-space resonance energy (angular frequency)  $\omega_0$ , and

$$\lambda^m(\omega, d) = 1 + \frac{6\pi c}{\omega} \text{Im} \hat{\mathbf{G}}_{mm}(d, d, \omega), \quad (10)$$

being the directional Purcell enhancement factor, when the transition dipole moment orientation of the QE is along the  $m$  axis ( $m = z, x$ ) and the location of the QE is at distance  $d$  above the center of the nanodisk. The probability amplitude evolution is obtained from the numerical solution of the above equation using the effective mode differential equation (EMDE) methodology [12].

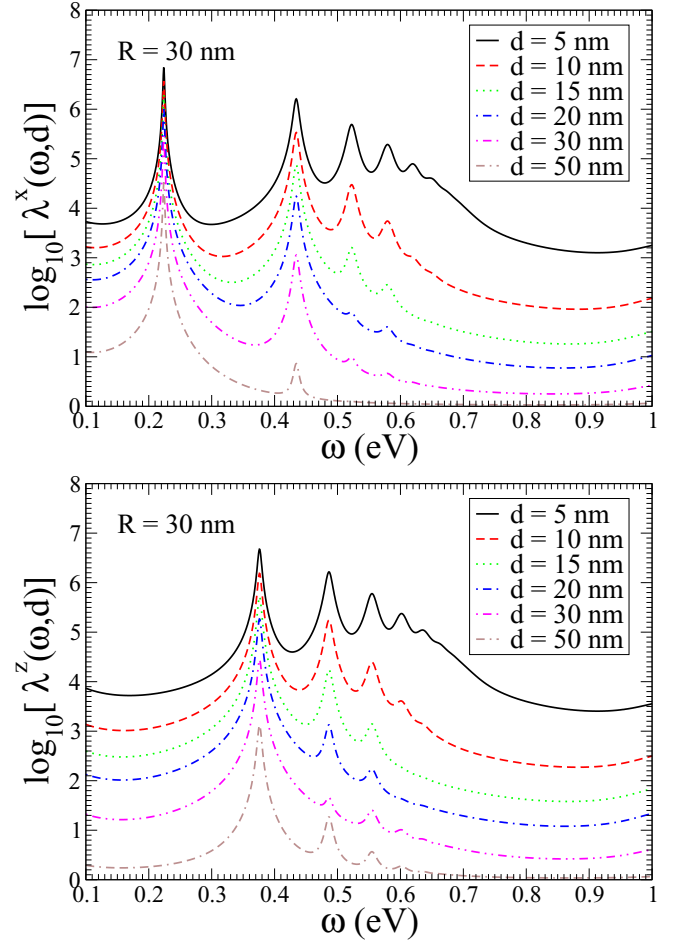


FIG. 2. The Purcell enhancement factor for a QE with transition dipole moment along the  $x$  axis (upper panel) and along the  $z$  axis (lower panel) at various distances from a graphene nanodisk of radius  $R = 30$  nm.

### III. RESULTS AND DISCUSSION

In Fig. 2, we present the Purcell factors of a QE with a  $x$ -oriented (upper panel) and  $z$ -oriented (lower panel) transition dipole moment, at various distance values of  $d = 5, 10, 15, 20, 30, 50$  nm between the QE and a graphene nanodisk of radius  $R = 30$  nm. One clearly observes that the peak positions in the Purcell factor spectrum, which correspond to plasmon resonance modes of the graphene nanodisk, depend on the transition dipole moment orientation of the QE, but remain practically unaffected by the QE and nanodisk separation distance. The two transition dipole moments of the QE excite different set of resonances. The peak value is, however, affected by the distance  $d$ ; expectedly, the Purcell enhancement factors decrease as the distance  $d$  grows.

In Fig. 3, we show the Purcell enhancement factor of a QE with  $z$ -oriented (lower panel) and  $x$ -oriented (upper panel) transition dipole moment located at  $d = 10$  nm from graphene nanodisks of various radii  $R = 7.5, 30, 50$  nm. We observe that the peak positions in the Purcell enhancement factor spectrum depend on the nanodisk radius, being redshifted as the radius grows. Moreover, we observe that as the radius of the nanodisk increases, the number of resonance peaks

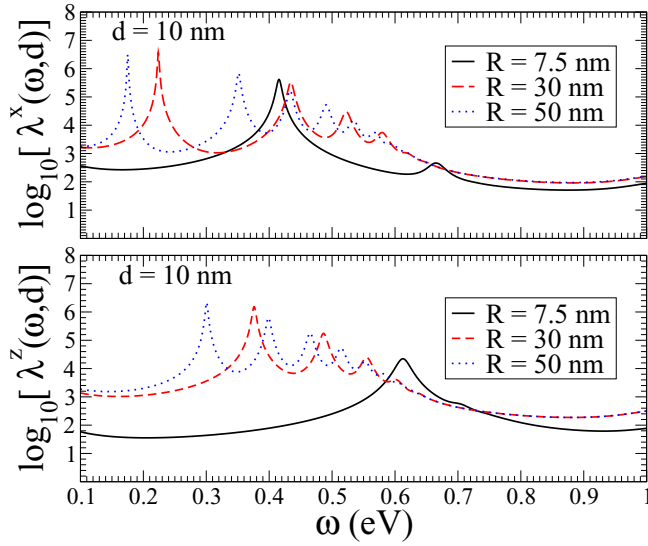


FIG. 3. The Purcell enhancement factor for a QE with transition dipole moment along the  $x$  axis (upper panel) and along the  $z$  axis (lower panel) at distance  $d = 10$  nm from a graphene nanodisk of various radii.

also increases due to the fact that the higher-order resonance modes can be supported in the larger nanodisk. Also, the near field of the QE couples stronger with the larger disk leading to higher Purcell factor values.

In the following, we present the spontaneous emission dynamics of a QE next to a graphene disk of radius  $R = 30$  nm under various coupling strength conditions between the QE and the nanodisk. We also study the non-Markovianity of the spontaneous emission process under these conditions by computing three well-established non-Markovianity measures and relate them to the quantum speedup of the corresponding dynamics.

In Fig. 4 we present the spontaneous emission dynamics of a QE with transition frequency  $\omega_0 = 0.22379$  eV and  $x$ -oriented transition dipole moment for various free-space decay rates  $\Gamma_0$  in the range of  $0.0008$ – $41.36$   $\mu\text{eV}$ . In the upper panel of this figure, the QE is located at  $d = 5$  nm from the nanodisk, and in the lower panel, it is located at  $d = 15$  nm. In the inset of the upper panel of Fig. 4, we present the spontaneous emission dynamics for the largest  $\Gamma_0$ , which implies that in this case, the light-matter interaction strength between the QE and the electromagnetic mode continuum modified by the graphene nanodisk is the strongest between the cases presented since the coupling strength is directly proportional to the free-space decay width  $\Gamma_0$ . We find, that at such coupling conditions, the excited-state population at early times rapidly oscillates in part between the QE and the electromagnetic mode continuum, and gradually attains a steady nonzero value, about 30% of the initial population. This is a clear indication of (partial) population trapping in the QE, which can be attributed to the formation of a stationary superposition state between the QE and the electromagnetic mode continuum due to the very strong coupling between them [13]. Below, we discuss in detail several aspects of the population trapping effect.

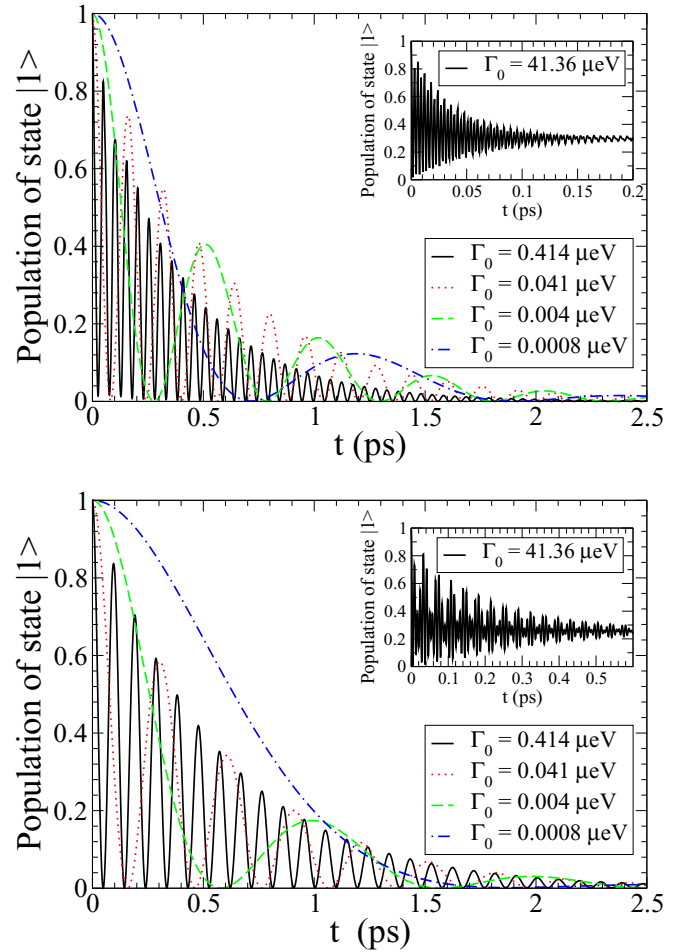


FIG. 4. Excited-state population dynamics for different  $\Gamma_0$  values for a QE with  $\omega_0 = 0.22379$  eV and  $x$ -oriented transition dipole moment located at  $d = 5$  nm (upper panel) and  $d = 15$  nm (lower panel) from a graphene nanodisk of  $R = 30$  nm.

In the main part of the upper panel of Fig. 4, we present the excited-state decay dynamics for smaller free-space decay widths, corresponding to weaker-coupling conditions between the QE and the electromagnetic mode continuum. In these cases, no partial population trapping is observed; however, clear decaying Rabi oscillations are found where the excited-state population oscillates in total back and forth between the electromagnetic mode continuum and the QE, whereas overall it gradually wanes out within about 2–2.5 ps. Thus, we conclude that the observed spontaneous emission dynamics in all such cases is distinctly non-Markovian.

In the main part and in the inset of the lower panel of Fig. 4, the spontaneous emission dynamics is similar to the corresponding dynamics shown in the upper panel of this figure when one takes into account that the Purcell enhancement factor along the  $x$  axis for a QE located at  $d = 15$  nm is smaller than when located at  $d = 5$  nm as shown in Fig. 2. In the inset of this panel, we observe again population trapping of about 25% of the initial population, whereas in all cases, but the smallest  $\Gamma_0$ , the spontaneous emission dynamics has non-Markovian features with pronounced decaying Rabi oscillations indicating the strong coupling between the

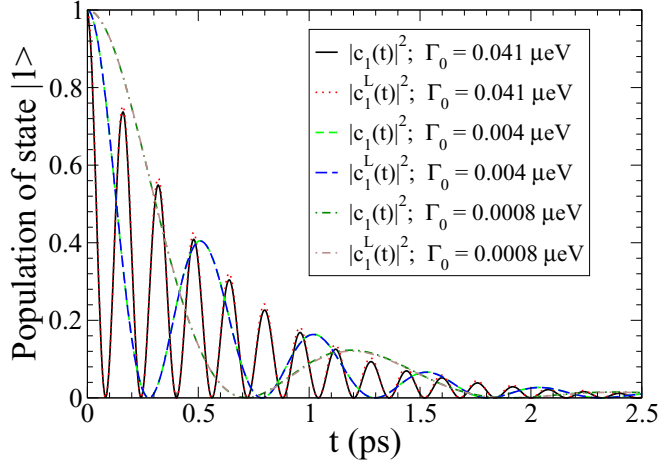


FIG. 5. Comparison of the excited-state population dynamics obtained with the EMDE method and analytically using Eq. (12) for different  $\Gamma_0$  values of a QE with  $\omega_0 = 0.22379$  eV and  $x$ -oriented transition dipole moment located at  $d = 5$  nm from a graphene nanodisk of  $R = 30$  nm.

QE and the electromagnetic mode continuum. In case when  $\Gamma_0 = 0.0008$   $\mu\text{eV}$ , although, the coupling has decreased significantly when the QE is at  $d = 15$  nm resulting in dynamics with weak non-Markovian features.

We may obtain an approximate analytical solution for the excited-state probability amplitude when the spectral density  $J(\omega)$  is approximated by a Lorentzian function [73],

$$J^L(\omega) = \frac{1}{2\pi} \frac{\Gamma_0(\omega_0)\lambda(\omega_0, d)\beta^2}{(\omega_0 - \omega - \Delta)^2 + \beta^2}, \quad (11)$$

where  $\Delta \equiv \omega_0 - \omega_c$  describes the detuning between the QE frequency  $\omega_0$  and a cavitylike central mode frequency  $\omega_c$ . Also,  $\beta$  denotes the spectral width of the coupling to the central mode. Taking the limit of the integral in Eq. (9) to  $-\infty$  and using the Laplace transform, it follows that the upper level probability amplitude of the QE is obtained as

$$c_1^L(t) = e^{-0.5\tilde{\beta}t} \left[ \cosh\left(\frac{qt}{2}\right) + \frac{\tilde{\beta}}{q} \sinh\left(\frac{qt}{2}\right) \right], \quad (12)$$

with  $q = \sqrt{\tilde{\beta}^2 - 2\Gamma_0(\omega_0)\lambda(\omega_0, d)\beta}$  and  $\tilde{\beta} = \beta - i\Delta$ .

In Fig. 5, we compare the spontaneous emission dynamics obtained using the exact EMDE method for cases presented in Fig. 4 for which the QE population decays totally with the analytically obtained dynamics according to Eq. (12) using the corresponding fitting parameters [74]. Apparently, the agreement between the EMDE method and the analytical result is very good, which clearly means that the excited-state population dynamics at this transition frequency is mainly affected by the corresponding peak in the Purcell enhancement factor as shown in Fig. 2, and the decaying Rabi oscillations reflect the dynamics between the bound state and the one resonance in the Purcell spectrum; moreover, this fact clearly indicates the absence of any influence of overlapping resonances in the Purcell spectrum on the decay dynamics. Also, this result confirms that for these system parameters the non-Hermitian Jaynes-Cummings model is validly justified for the study of

the spontaneous emission dynamics of the QE near a graphene nanodisk [8,73].

We now turn our attention to the population trapping effect, which cannot be predicted by the non-Hermitian Jaynes-Cummings model [13,19], and explore the formation of a hybrid stationary bound state. A semianalytical estimate for the value of the trapped population when such a bound state  $|\psi_B\rangle$  is formed can be derived by writing

$$|\psi_B\rangle = c_{1B}|1, 0_{z,\omega}\rangle + \int d\mathbf{r} \int d\omega C_B(\mathbf{r}, \mathbf{r}_1, \omega)|0, 1_{z,\omega}\rangle, \quad (13)$$

where  $c_{1B}$  and  $C_B$  are the time-independent population coefficients. Since  $|\psi_B\rangle$  obeys the Schrödinger equation  $H|\psi_B\rangle = \omega_B|\psi_B\rangle$ , we obtain two secular equations,

$$\omega_B c_{1B} = \omega_0 c_{1B} + \int d\omega \int d\mathbf{r} g(\mathbf{r}, \mathbf{r}', \omega) C_B(\mathbf{r}, \mathbf{r}', \omega), \quad (14)$$

$$\omega_B C_B(\mathbf{r}, \mathbf{r}', \omega) = \omega_0 C_B(\mathbf{r}, \mathbf{r}_1, \omega) + g^\dagger(\mathbf{r}, \mathbf{r}', \omega) c_{1B}. \quad (15)$$

Hybrid bound states would appear if the secular equations have solutions that lie outside the energy spectrum of the EM continuum of modes as modified by the presence of a nanostructure [75]. Using the above two equations we extract the relation  $\omega_B - \omega_0 - \int_0^\infty d\omega \frac{J(\omega)}{\omega_B - \omega} = 0$  as a such hybrid bound state formation requirement; we further define the function,

$$f(\omega_B) = \omega_B - \omega_0 - \int_0^\infty d\omega \frac{J(\omega)}{\omega_B - \omega}, \quad (16)$$

which for  $f(\omega_B) = 0$  and  $\omega_B < 0$ , the system under consideration has a bound state. The integral is a monotonically increasing function, thus, there is only one point that can satisfy the above condition in the relevant energy range of  $(-\infty, 0]$ . The time evolution of a state describing the QE being initially excited and the electromagnetic field modified by the graphene nanodisk in the ground state,  $|\Psi(0)\rangle = |e, \{0_{\mathbf{r},\omega}\}\rangle$  follows  $|\Psi(t)\rangle = c_{1B}e^{-i\omega_B t}|\Phi_B\rangle$ , with  $c_{1B} = \langle\Phi_B|\Psi(0)\rangle$  at  $t = 0$ . The overlap with the system initial state is given by  $\langle\Psi(0)|\Psi(t)\rangle = |c_{1B}|^2 e^{-i\omega_B t}$ .

From Eq. (14), and the normalization condition  $\langle\psi_B|\psi_B\rangle = 1$ , the population coefficients satisfy the relation,

$$|c_{1B}|^2 + \int d\omega \int d\mathbf{r} |C_B(\mathbf{r}, \mathbf{r}', \omega)|^2 = 1. \quad (17)$$

Thus, the QE population for  $t \rightarrow \infty$  when a bound state is formed, is given by

$$P_B = \left[ 1 + \int_0^\infty d\omega \frac{J(\omega)}{(\omega_B - \omega)^2} \right]^{-2}. \quad (18)$$

Application of Eq. (18) to the cases with the largest  $\Gamma_0$ 's in the insets of the upper and lower panels of Fig. 4 gives  $P_B = 0.296$  and  $P_B = 0.256$ , respectively, which is in very good agreement with the obtained numerical values shown using the exact EMDE methodology.

We further investigate the non-Markovian behavior of the spontaneous emission dynamics of the QE by using different non-Markovianity measures [63,64] for the interaction between the QE and the electromagnetic continuum which is modified by the presence of the graphene nanodisk. We use three measures for the non-Markovianity of the quantum

TABLE I. Non-Markovianity measure values [63,64] for various  $\Gamma_0$ 's of a QE with a  $x$ -oriented transition dipole moment located at  $d = 5$  and  $d = 15$  nm from a graphene nanodisk of radius  $R = 30$  nm.

$\Gamma_0/\mu\text{eV}$	$d = 5$ nm			$d = 15$ nm		
	$\mathcal{N}$	$\mathcal{I}^E$	$\mathcal{I}$	$\mathcal{N}$	$\mathcal{I}^E$	$\mathcal{I}$
41.36	14.2	26.12	51.63	16.64	33.04	71.49
0.414	12.44	24.89	272.70	9.11	18.22	125.71
0.041	5.45	10.89	131.54	2.82	5.64	62.34
0.004	1.51	3.02	33.52	0.561	1.12	11.74
0.0008	0.43	0.86	9.21	0.06	0.12	1.83

evolution. The BLP measure  $\mathcal{N}$  as defined in Ref. [63] and the two RHP measures  $\mathcal{I}^E$  and  $\mathcal{I}$  as defined in Ref. [64]. We note that Ref. [76] showed that these three non-Markovianity measures are equivalent when they are used in the case of a two-level QE interacting with a photonic environment via a frequency-dependent coupling.

For the calculations, we first obtain the time-dependent decay rate,

$$\gamma(t) = -2 \operatorname{Re} \left( \frac{\dot{c}_1(t)}{c_1(t)} \right) = -\frac{2}{|c_1(t)|} \frac{d}{dt} |c_1(t)|, \quad (19)$$

and then determine the function,

$$F(t, a, b) = \frac{a^2 e^{-(3/2)\Gamma(t)} + |b|^2 e^{-(1/2)\Gamma(t)}}{\sqrt{a^2 e^{-\Gamma(t)} + |b|^2}}, \quad (20)$$

where

$$\Gamma(t) = \int_0^t dt' \gamma(t'). \quad (21)$$

Here,

$$a = \langle 1|\rho_1(0)|1\rangle - \langle 1|\rho_2(0)|1\rangle \quad (22)$$

is the difference of the populations and

$$b = \langle 1|\rho_1(0)|0\rangle - \langle 1|\rho_2(0)|0\rangle \quad (23)$$

is the difference of the coherences between two arbitrary initial states.

Using the above formulas, the BLP measure [63] is obtained by

$$\mathcal{N} = -\max_{a,b} \int_{\gamma(t)<0} \gamma(t) F(t, a, b) dt \quad (24)$$

for  $F(t, a, b)$  with fixed values for  $a$  and  $b$ . Also, the RHP measures [64] are given by

$$\mathcal{I}^E = -\int_{\gamma(t)<0} \gamma(t) e^{-(1/2)\Gamma(t)} dt, \quad (25)$$

and

$$\mathcal{I} = -\int_{\gamma(t)<0} \gamma(t) dt. \quad (26)$$

In Table I we present the values for the  $\mathcal{N}$ ,  $\mathcal{I}^E$ , and  $\mathcal{I}$  non-Markovianity measures, noting that the values among the three measures are not comparable since each value is not normalized. As a general trend, we observe that the value

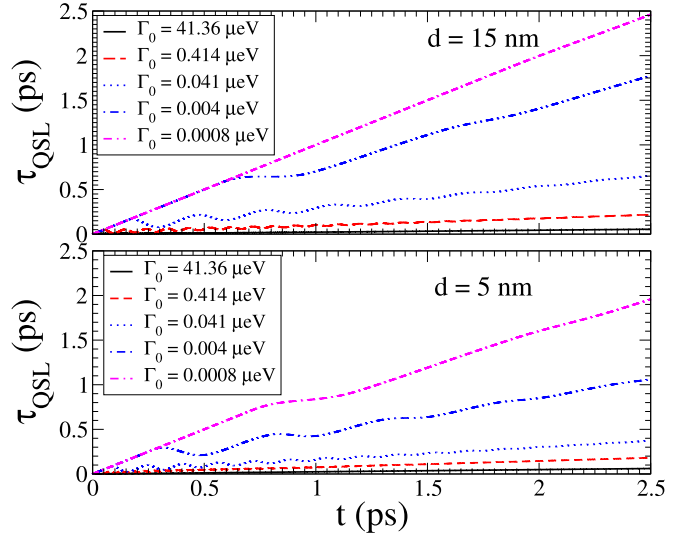


FIG. 6. Quantum speed limit  $\tau_{\text{QSL}}$  for the spontaneous emission dynamics of a QE with  $\omega_0 = 0.22379$  eV with  $x$ -oriented dipole moment located at  $d = 5$  nm (lower panel) and  $d = 15$  nm (upper panel) from a graphene disk of radius  $R = 30$  nm.

of each measure increases as the coupling strength between the QE and the graphene nanodisk increases. We, however, note that the values of the measures might decrease as the oscillation period of the population dynamics become shorter since all three measure definitions consider only the part of the dynamics for which  $\gamma(t) < 0$ . This is the case, in particular, for the  $\mathcal{I}$  measure, which is just the sum of such intervals, under population trapping coupling conditions; thus, in such a case, its value is not anymore directly related to the coupling strength.

In Fig. 6 we further present the quantum speed limit  $\tau_{\text{QSL}}$  for the spontaneous emission dynamics of a QE with  $\omega_0 = 0.22379$  eV located at  $d = 5$  nm (lower panel) and  $d = 15$  nm (upper panel) from a  $R = 30$ -nm graphene nanodisk. The quantum speed limit places a bound on the minimal evolution of an open quantum system [65]. It has been shown that the quantum speed limit can be related to the non-Markovianity of the open quantum system dynamics by [77]

$$\tau_{\text{QSL}} = \frac{t}{2 \frac{\tilde{N}(t)}{1-|c_1(t)|^2} + 1}, \quad (27)$$

with

$$\tilde{N}(t) = 0.5 \int_0^t |\partial_{t'} [c_1(t') c_1^*(t')] | dt' + [c_1(t) c_1^*(t)] - 1, \quad (28)$$

where  $t$  is the actual driving time of the open quantum system. From Eq. (27) is evident that the quantum speed limit is identical to the actual driving time when  $\tilde{N} = 0$ , which implies Markovian dynamics. In all other cases, the quantum speed limit always attains a smaller value than the driving time, indicating that by exploiting the non-Markovianity of an open quantum system one can obtain a speedup of the actual quantum dynamics in comparison to the corresponding dynamics under Markovian conditions.

We now focus on the spontaneous emission dynamics of a QE with a  $z$ -oriented transition dipole moment and  $\omega_0 =$

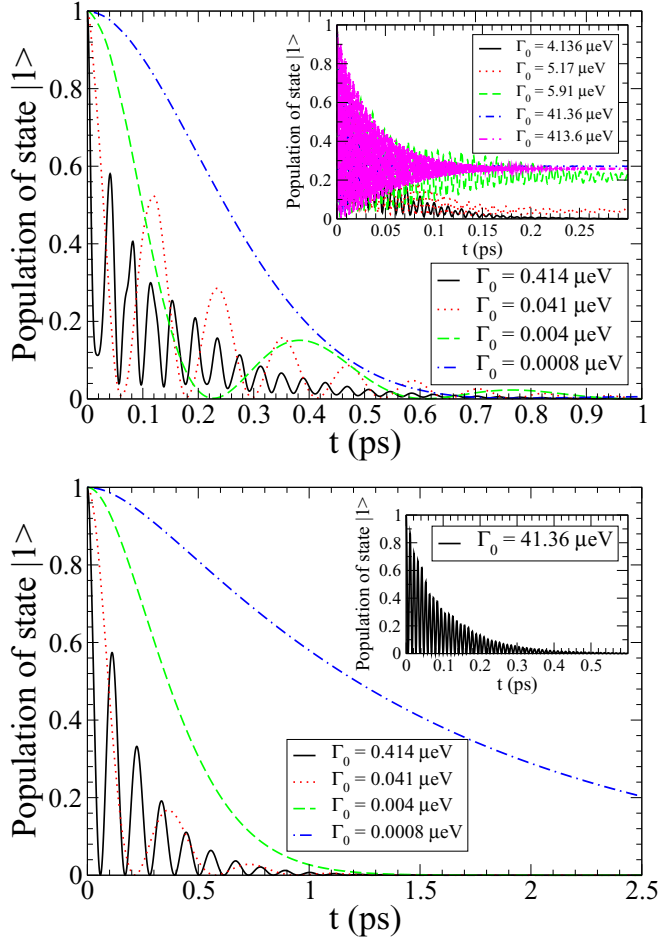


FIG. 7. Excited-state population dynamics for different  $\Gamma_0$  values for a QE with transition energy 0.375 83 eV and  $z$ -oriented transition dipole moment located at  $d = 5$  nm (upper panel) and  $d = 15$  nm (lower panel) from a graphene nanodisk of  $R = 30$  nm.

0.375 83 eV next to a graphene nanodisk of radius  $R = 30$  nm. In Fig. 7 we present the results in case of a QE located at  $d = 5$  and  $d = 15$  nm, which are shown in the upper and lower panels, respectively. The spontaneous emission dynamics of the QE at  $d = 5$  nm is similar to the corresponding results for a QE with  $x$ -oriented transition dipole moment shown in the upper panel of Fig. 4. The main difference in the dynamics between the two transition dipole polarization cases is that in case of a QE with  $z$ -oriented transition dipole, the excited-state population decays oscillating back and forth between the QE and the electromagnetic continuum with larger period and showing incomplete oscillations than in case of a QE with a  $x$ -oriented transition dipole moment. This fact can be related to the small overlap of the Purcell enhancement peak at  $\omega_0 = 0.375$  83 eV with the next peak with higher energy in the Purcell enhancement spectrum. Note that the peak in the Purcell spectrum which is resonant to the QE with  $\omega_0 = 0.375$  83 eV is not as energetically distant to the next higher-energy peak in the spectrum as in the case of a QE with  $\omega_0 = 0.223$  79 eV shown in Fig. 2.

In Fig. 7 population trapping occurs when the QE is located at  $d = 5$  nm from the graphene disk. The corresponding

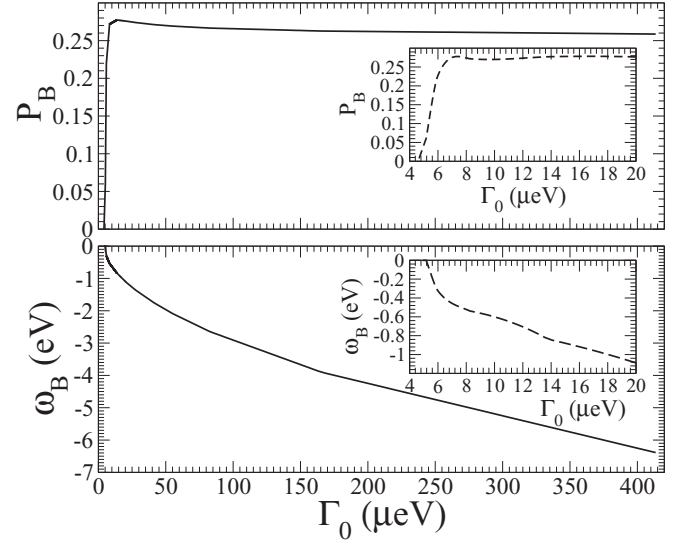


FIG. 8. Trapped-population  $P_B$  and corresponding hybrid bound-state frequency  $\omega_B$  for the spontaneous emission dynamics of a QE with  $\omega_0 = 0.375$  83 eV with the  $z$ -oriented dipole moment located at  $d = 5$  nm from a graphene disk of radius  $R = 30$  nm for various decay width values  $\Gamma_0$ .

excited-state population time-evolution features incomplete oscillations of the initial population of the QE back and forth to the graphene nanodisk-modified electromagnetic mode continuum until it gradually attains a constant value, which reflects the amount of trapped population in the excited state of the QE. The oscillatory features of the initial part of the spontaneous emission dynamics can be understood as interference effects due to the overlapping resonances in the corresponding Purcell spectrum, or, alternatively, as interference between an overlapping bound state outside the continuum and a bound state at the energetically lowest continuum edge as discussed in Ref. [78].

Interestingly, we observe that the population trapping effect does not behave linearly to the decay width  $\Gamma_0$ , although the coupling strength of the light-matter interaction does. This fact is demonstrated by the QE decay dynamics presented in the inset of the upper panel of Fig. 7, where, e.g., a small change in  $\Gamma_0$  from 5.17 to 5.91  $\mu\text{eV}$ , i.e., an increase in 14.3% of  $\Gamma_0$ , leads to the value of the trapped population in the system being increased from about 0.06 to 0.22, about 267%. Furthermore, in the same inset it is shown, that after some particular value of  $\Gamma_0$ , the amount of trapped population remains practically the same, even if the  $\Gamma_0$ , and, correspondingly, the coupling strength of the interaction, increases by even an order of magnitude.

Additionally, in Fig. 8 we present the trapped-population  $P_B$  (upper panel), obtained by Eq. (18), and corresponding hybrid bound state frequency  $\omega_B$  (lower panel) for the spontaneous emission dynamics of a QE with  $\omega_0 = 0.375$  83 eV with  $z$ -oriented dipole moment located at  $d = 5$  nm from a graphene disk of radius  $R = 30$  nm as function of the decay width values  $\Gamma_0$ . It is clearly shown that increasing the  $\Gamma_0$ , and, thus, the light-matter coupling between the QE and the graphene nanodisk, the  $\omega_B$  decreases correspondingly, indicating the formation of a bound state energetically farther

TABLE II. Non-Markovianity measure values [63,64] for various  $\Gamma_0$ 's of a QE with a  $z$ -oriented transition dipole moment located at  $d = 5$  and  $d = 15$  nm from a graphene nanodisk of radius  $R = 30$  nm.

$\Gamma_0/\mu\text{eV}$	$d = 5$ nm			$d = 15$ nm		
	$\mathcal{N}$	$\mathcal{I}^{(E)}$	$\mathcal{I}$	$\mathcal{N}$	$\mathcal{I}^{(E)}$	$\mathcal{I}$
41.36	7.85	15.19	33.52	18.32	36.65	843.32
0.414	3.17	6.33	37.08	3.10	6.20	141.70
0.041	2.31	4.62	54.07	0.65	1.30	33.19
0.004	0.54	1.09	17.92	0	0	0
0.0008	0.03	0.07	1.36	0	0	0

outside the continuum. Moreover, we find that the relation between the decay width and the bound-state energy is for the largest part of the  $\Gamma_0$  range linear. However, this is not the case between the  $\Gamma_0$  and the trapped population value  $P_B$  as shown in the upper panel of Fig. 8 in which it is shown that  $P_B$  grows very fast as the decay width grows up to a value that remains practically unaffected as  $\Gamma_0$  grows further. Such a nonlinear behavior between the amount of trapped population and the  $\Gamma_0$  have been observed (not shown here) also in all previous cases of spontaneous emission dynamics discussed in this paper. It is also in agreement with recent theoretical and experimental works [79,80].

Lastly, in Table II we present the values for the  $\mathcal{N}$ ,  $\mathcal{I}^E$ , and  $\mathcal{I}$  non-Markovianity measures for the spontaneous emission dynamics of a QE with  $z$ -oriented transition dipole moment shown in Fig. 7. Here, as earlier, the values of the measures are directly related to the coupling strength of the interaction between the QE and the nanodisk in all cases except under population trapping conditions. The comparison of the measure values given in Table II to the corresponding measure values shown in Table I clearly indicate that the decay dynamics of the QE with a  $z$ -oriented transition dipole moment has less non-Markovian features, which implies weaker coupling between the QE and the electromagnetic continuum, than in case of a QE with a  $x$ -oriented transition dipole moment.

#### IV. CONCLUSIONS

In this paper, we studied the spontaneous emission dynamics of a QE near a graphene nanodisk. We analyzed the re-

versible excited-state population dynamics and quantified the non-Markovian behavior using different non-Markovianity measures. We also related the non-Markovianity of the evolution dynamics with the quantum speed limit, which can be achieved under the given coupling conditions.

In particular, we investigated the spontaneous emission dynamics of the excited-state population of a QE modeled as a two-level system located at 5 and 15 nm from a graphene nanodisk of radius 30 nm, whereas the free-space decay time of the emitter lies between 100 ps and microseconds. We find that at a close distance and under short free-space decay times of the QE, the observed dynamics shows strong non-Markovian features, depending on the distance among the QE, the graphene nanodisk, and the free-space spontaneous decay rate. As the distance from the nanodisk or the free-space decay time increases, the non-Markovian features in the dynamics diminish. These findings reflect the transition from conditions under strong light-matter coupling to weak coupling. Under strong-coupling conditions, we also observe pronounced decaying Rabi oscillations and population trapping effects in the dynamical evolution of the excited-state population of the QE.

We also quantified the non-Markovianity of the spontaneous emission dynamics by computing different measures as well as the quantum speed limit for each case. These results are in agreement with the behavior of the QE excited-state population dynamics under strong-coupling conditions, giving large measure values and potentially large quantum speedup for the dynamics under such coupling conditions, whereas both properties are decreasing as the coupling diminishes. In conclusion, it is evident that the graphene nanodisk can become a platform for achieving strong-coupling conditions for light-matter interaction at the nanoscale even for large free-space decay times and at long distances between the quantum emitter and the nanophotonic structure when compared to the metallic nanostructures.

#### ACKNOWLEDGMENTS

We gratefully acknowledge invaluable help and stimulating discussions with Prof. A. G. Vanakaras. E.P. acknowledges partial financial support by the Horizon-2020 Research and Innovation Program of the European Union (Grant No. 952335, NanoQIQO Project).

- 
- [1] M. S. Tame, K. R. McEnery, S. K. Özdemir, J. Lee, S. A. Maier, and M. S. Kim, *Nat. Phys.* **9**, 329 (2013).
  - [2] D. G. Baranov, M. Wersäll, J. Cuadra, T. J. Antosiewicz, and T. Shegai, *ACS Photonics* **5**, 24 (2018).
  - [3] B. Kolaric, B. Maes, K. Clays, T. Durt, and Y. Caudano, *Adv. Quantum Technol.* **1**, 1800001 (2018).
  - [4] J. Flick, N. Rivera, and P. Narang, *Nanophotonics* **7**, 1479 (2018).
  - [5] A. I. Fernández-Domínguez, S. I. Bozhevolnyi, and N. Asger Mortensen, *ACS Photonics* **5**, 3447 (2018).
  - [6] O. Bitton, S. N. Gupta, and G. Haran, *Nanophotonics* **8**, 559 (2019).
  - [7] V. Karanikolas, S. Suzuki, S. Li, and T. Iwasaki, *Appl. Phys. Lett.* **120**, 040501 (2022).
  - [8] A. Gonzalez-Tudela, P. A. Huidobro, L. Martin-Moreno, C. Tejedor, and F. J. Garcia-Vidal, *Phys. Rev. B* **89**, 041402(R) (2014).
  - [9] J. Hakami, L. Wang, and M. S. Zubairy, *Phys. Rev. A* **89**, 053835 (2014).
  - [10] H. Varguet, B. Rousseaux, D. Dzsofjan, H. R. Jauslin, S. Guérin, and G. Colas des Francs, *Opt. Lett.* **41**, 4480 (2016).
  - [11] R.-Q. Li, D. Hernangomez-Perez, F. J. Garcia-Vidal, and A. I. Fernandez-Dominguez, *Phys. Rev. Lett.* **117**, 107401 (2016).

- [12] I. Thanopoulos, V. Yannopoulos, and E. Paspalakis, *Phys. Rev. B* **95**, 075412 (2017).
- [13] C.-J. Yang and J.-H. An, *Phys. Rev. B* **95**, 161408(R) (2017).
- [14] R.-Q. Li, F. J. Garcia-Vidal, and A. I. Fernandez-Dominguez, *ACS Photonics* **5**, 177 (2018).
- [15] M. Hensen, T. Heilpern, S. K. Gray, and W. Pfeiffer, *ACS Photonics* **5**, 240 (2018).
- [16] T. Neuman, R. Esteban, D. Casanova, F. J. Garcia-Vidal, and J. Aizpurua, *Nano Lett.* **18**, 2358 (2018).
- [17] A. Cuartero-González and A. I. Fernandez-Dominguez, *ACS Photonics* **5**, 3415 (2018).
- [18] B. Rousseaux, D. G. Baranov, M. Käll, T. Shegai, and G. Johansson, *Phys. Rev. B* **98**, 045435 (2018).
- [19] C.-J. Yang, J.-H. An, and H.-Q. Lin, *Phys. Rev. Res.* **1**, 023027 (2019).
- [20] S. Wang, G. D. Scholes, and L.-Y. Hsu, *J. Chem. Phys.* **151**, 014105 (2019).
- [21] M. Tian, Y.-G. Huang, S.-S. Wen, X.-Y. Wang, H. Yang, J.-Z. Peng, and H.-P. Zhao, *Phys. Rev. A* **99**, 053844 (2019).
- [22] S.-S. Wen, Y.-G. Huang, X.-Y. Wang, J. Liu, Y. Li, X.-E. Quan, H. Yang, J.-Z. Peng, K. Deng, and H.-P. Zhao, *Opt. Express* **28**, 6469 (2020).
- [23] M.-W. Lee, Y.-T. Chuang, and L.-Y. Hsu, *J. Chem. Phys.* **155**, 074101 (2021).
- [24] S. Wang, Y.-T. Chuang, and L.-Y. Hsu, *J. Chem. Phys.* **155**, 134117 (2021).
- [25] V. Karanikolas, I. Thanopoulos, J. D. Cox, T. Kuroda, J.-I. Inoue, N. A. Mortensen, E. Paspalakis, and C. Tserkezis, *Phys. Rev. B* **104**, L201405 (2021).
- [26] R. Chikkaraddy, B. Nijs, F. Benz, S. J. Barrow, O. A. Scherman, E. Rosta, A. Demetriadou, P. Fox, O. Hess, and J. J. Baumberg, *Nature (London)* **535**, 127 (2016).
- [27] K. Santhosh, O. Bitton, L. Chuntonov, and G. Haran, *Nat. Commun.* **7**, ncomms11823 (2016).
- [28] R. Liu, Z.-K. Zhou, Y.-C. Yu, T. Zhang, H. Wang, G. Liu, Y. Wei, H. Chen, and X.-H. Wang, *Phys. Rev. Lett.* **118**, 237401 (2017).
- [29] Y. Zhang, Q.-S. Meng, L. Zhang, Y. Luo, Y.-J. Yu, B. Yang, Y. Zhang, R. Esteban, J. Aizpurua, Y. Luo, J.-L. Yang, Z.-C. Dong, and J. G. Hou, *Nat. Commun.* **8**, 15225 (2017).
- [30] T. Low and P. Avouris, *ACS Nano* **8**, 1086 (2014).
- [31] F. J. García de Abajo, *ACS Photonics* **1**, 135 (2014).
- [32] F. H. L. Koppens, D. E. Chang, and F. J. García de Abajo, *Nano Lett.* **11**, 3370 (2011).
- [33] J. D. Cox, M. R. Singh, G. Gumbs, M. A. Antón, and F. Carreño, *Phys. Rev. B* **86**, 125452 (2012).
- [34] A. Manjavacas, P. Nordlander, and F. J. García de Abajo, *ACS Nano* **6**, 1724 (2012).
- [35] S.-A. Biehs and G. S. Agarwal, *Appl. Phys. Lett.* **103**, 243112 (2013).
- [36] E. Forati, G. W. Hanson, and S. Hughes, *Phys. Rev. B* **90**, 085414 (2014).
- [37] L. Sun, B. Tang, and C. Jiang, *Opt. Express* **22**, 26487 (2014).
- [38] V. D. Karanikolas, C. A. Marocico, and A. L. Bradley, *Phys. Rev. B* **91**, 125422 (2015).
- [39] V. D. Karanikolas, C. A. Marocico, and A. L. Bradley, *Phys. Rev. B* **93**, 035426 (2016).
- [40] M. Cuevas, M. A. Riso, and R. A. Depine, *J. Quant. Spectrosc. Radiat. Transfer* **173**, 26 (2016).
- [41] N. Rivera, I. Kaminer, B. Zhen, J. D. Joannopoulos, and M. Soljačić, *Science* **353**, 263 (2016).
- [42] C.-H. Chang, N. Rivera, J. D. Joannopoulos, M. Soljačić, and I. Kaminer, *ACS Photonics* **4**, 3098 (2017).
- [43] L. Sun, G. Zhang, S. Zhang, and J.-H. Ji, *Opt. Express* **25**, 14270 (2017).
- [44] M. Cuevas, *J. Quant. Spectrosc. Radiat. Transfer* **206**, 157 (2018).
- [45] J. Sloan, N. Rivera, M. Soljačić, and I. Kaminer, *Nano Lett.* **18**, 308 (2018).
- [46] V. Karanikolas and E. Paspalakis, *J. Phys. Chem. C* **122**, 14788 (2018).
- [47] Y.-X. Zhang, Y. Zhang, and K. Mølmer, *Phys. Rev. A* **98**, 033821 (2018).
- [48] S. Sanders, A. May, A. Alabastri, and A. Manjavacas, *ACS Photonics* **5**, 3282 (2018).
- [49] W. Fang, G.-X. Li, and Y. P. Yang, *Opt. Express* **26**, 29561 (2018).
- [50] J. D. Cox and F. J. García de Abajo, *Phys. Rev. Lett.* **121**, 257403 (2018).
- [51] J. Olivo, C. J. Zapata-Rodríguez, and M. Cuevas, *J. Opt.* **21**, 045002 (2019).
- [52] X.-D. Zeng, Z.-H. Li, G.-Q. Ge, and M. S. Zubairy, *Phys. Rev. A* **99**, 043811 (2019).
- [53] Y.-X. Zhang, Y. Zhang, and K. Mølmer, *ACS Photonics* **6**, 871 (2019).
- [54] V. Karanikolas, P. Tozman, and E. Paspalakis, *Phys. Rev. B*, **100**, 245403 (2019).
- [55] X.-D. Zeng and M. S. Zubairy, *Phys. Rev. Lett.* **126**, 117401 (2021).
- [56] M. R. Singh, M. J. Brzozowski, and B. Apter, *J. Appl. Phys.* **120**, 124308 (2016).
- [57] M. J. Brzozowski and M. R. Singh, *Plasmonics* **12**, 1021 (2017).
- [58] H. T. Dung, L. Knöll, and D.-G. Welsch, *Phys. Rev. A* **62**, 053804 (2000).
- [59] I. Thanopoulos, V. Karanikolas, N. Iliopoulos, and E. Paspalakis, *Phys. Rev. B* **99**, 195412 (2019).
- [60] N. Iliopoulos, V. Karanikolas, I. Thanopoulos, and E. Paspalakis, *Physica E* **119**, 113967 (2020).
- [61] I. Thanopoulos, K. Blekos, P. Kalozoumis, V. Karanikolas, and E. Paspalakis, *Physica E* **133**, 114780 (2021).
- [62] F.-Z. Ji, S.-Y. Bai, and J.-H. An, *arXiv:2204.13383*.
- [63] H.-P. Breuer, E.-M. Laine, and J. Piilo, *Phys. Rev. Lett.* **103**, 210401 (2009).
- [64] A. Rivas, S. F. Huelga, and M. B. Plenio, *Phys. Rev. Lett.* **105**, 050403 (2010).
- [65] S. Deffner and E. Lutz, *Phys. Rev. Lett.* **111**, 010402 (2013).
- [66] C. W. Hsu, B. Zhen, A. D. Stone, J. D. Joannopoulos, and M. Soljačić, *Nat. Rev. Mater.* **1**, 16048 (2016).
- [67] S. Longhi, *Eur. Phys. J. B* **57**, 45 (2007).
- [68] M. Jablan, H. Buljan, and M. Soljačić, *Phys. Rev. B* **80**, 245435 (2009).
- [69] L. A. Falkovsky, *J. Phys.: Conf. Ser.* **129**, 012004 (2008).
- [70] B. Wunsch, T. Stauber, F. Sols, and F. Guinea, *New J. Phys.* **8**, 318 (2006).
- [71] K. S. Novoselov, *Science* **306**, 666 (2004).
- [72] A. L. Fetter, *Phys. Rev. B* **33**, 5221 (1986).

- [73] H.-P. Breuer and F. Petruccione, *The Theory of Open Quantum Systems* (Oxford University Press, Oxford, UK, 2002).
- [74] The fitting procedure for a graphene nanodisk of  $R = 30$ -nm radius results in  $\beta = 1.17 \times 10^{-3} \pm 1.096 \times 10^{-6}$  eV for  $\omega_c = 0.223787$  eV by applying a single peak fitting to  $J(\omega)$  using  $J^L(\omega)$ , independent of  $d$ .
- [75] T. Shi, Y.-H. Wu, A. González-Tudela, and J. I. Cirac, *Phys. Rev. X* **6**, 021027 (2016).
- [76] H.-S. Zeng, N. Tang, Y.-P. Zheng, and G.-Y. Wang, *Phys. Rev. A* **84**, 032118 (2011).
- [77] Z.-Y. Xu, S.-L. Luo, W. L. Yang, C. Liu, and S.-Q. Zhu, *Phys. Rev. A* **89**, 012307 (2014).
- [78] S. John and T. Quang, *Phys. Rev. A* **50**, 1764 (1994).
- [79] S. Garmon, H. Nakamura, N. Hatano, and T. Petrosky, *Phys. Rev. B* **80**, 115318 (2009).
- [80] Y. Liu and A. A. Houck, *Nat. Phys.* **13**, 48 (2017).